


OSA 2024

Numerical and Experimental Analysis of Tuning Three Selected Types of Acoustic Helicoidal Resonators with 90-Degree Duct Elbow

Wojciech ŁAPKA 

*Division of Vibroacoustics and Diagnostics of Systems, Institute of Applied Mechanics
Faculty of Mechanical Engineering, Poznan University of Technology
Poznań, Poland; e-mail: wojciech.lapka@put.poznan.pl*

This work presents the results of numerical and experimental analyses regarding the tuning of three selected acoustic helicoidal resonators using a 90-degree elbow in a cylindrical duct. The elbow is placed directly at the end of the resonators, which were additionally rotated about the duct axis at a specific angle (45° angle change in the numerical analysis and 90° angle change in the experiment). Three resonators with the same helicoid pitch-to-duct diameter ratio of $s/d = 1.976$ but with different numbers of turns n of 0.671, 0.695, and 1.0 were selected for analysis. They represent three different transmission loss (TL) characteristics in the frequency domain. In the considered system of helicoidal resonators and a 90-degree duct elbow, it was found that the selected resonators can be tuned by rotating them, effectively covering nearly the entire range of their characteristic sound attenuation resulting from acoustic resonance.

Keywords: helicoidal resonator; duct acoustics; experiment; numerical analysis.



Copyright © 2025 The Author(s).
Published by IPPT PAN. This work is licensed under the Creative Commons Attribution License
CC BY 4.0 (<https://creativecommons.org/licenses/by/4.0/>).

1. INTRODUCTION

Acoustic resonators, devices designed to enhance or attenuate specific frequencies through resonance, are fundamental tools in the field of acoustics. They are widely utilized in various applications [8], ranging from noise control in enclosures [7] to innovative acoustic metamaterials for advanced sound manipulation [5]. Precise tuning of these resonators is crucial for optimizing their performance, particularly in controlling narrowband noise and enhancing sound absorption in constrained environments.

The tuning of an acoustic resonator involves adjusting its Helmholtz frequency and internal resistance to achieve desired acoustic outcomes. This process is essential for effective narrowband noise control [1, 4, 6, 9, 10, 14, 26].

In this field, the specific solutions for the spiral neck of the Helmholtz resonator were considered [23], as well as extended [6, 22] and tapered neck solutions [24].

Based on the operating principles of the Helmholtz resonator [5], the concept of extended-tube acoustic metamaterials was investigated for practical applications [2]. This study presents an impedance model for a single-layer extended-tube structure, incorporating visco-thermal effects and flow-distortion corrections. The fabricated samples demonstrate superior noise reduction capabilities in confined spaces, such as kitchen hoods, compared to conventional materials. The structural simplicity and effectiveness of these extended-tube metamaterials highlight their potential for widespread adoption in noise-sensitive environments.

Research on acoustic helicoidal resonators has been ongoing for over 15 years and brings increasingly interesting results. Initially, what was fascinating was the discovery of the resonance properties of the helicoidal profile, initially observed in three turns with a specific pitch, and later extended to only one turn, or even its incomplete expansion. Subsequent studies started exploring various systems, and they focused on changing the pitch of the helicoid while leaving the diameter of the cylindrical duct constant [13]. At that time, the properties of resonators were examined only in a straight cylindrical duct. Changes in acoustic properties were determined by adjusting the mandrel diameter and profile thickness, and the possibilities for combining their properties with various standard noise silencers were determined [2, 13, 16]. The properties of the Helmholtz resonator were also compared with those of helicoidal resonators [14]. A number of aeroacoustic tests were performed, which resulted in the development of knowledge about the introduced pressure drop in the system and flow-induced noise [17, 18].

Numerical studies on the effect of placing a 90-degree bend at the end of a resonator with the helicoid pitch-to-duct diameter ratio $s/d = 1.976$ and one full turn $n = 1.0$ began in 2018 [15].

While some recent studies have investigated the acoustic performance of resonator arrays [10], genetic optimization of filter configurations [11], or metamaterial-based concepts [19], to the best of the author's knowledge, the coupling effect between helicoidal resonator geometry and duct elbow orientation has not yet been addressed. The present study aims to address this gap.

This work includes the development of numerical studies for three helicoidal resonators with turn numbers n of 0.671, 0.695, and 1.0 with 90-degree duct elbow rotations about their axes in 45-degree steps. This work also includes experimental validation of placing a standard 90-degree elbow in a commercially available 125 mm diameter duct, with rotations about their axes in 90-degree steps.

The acoustic impedance and end-correction effects introduced by duct geometry are critical in determining a resonator's performance. These parameters sig-

nificantly influence the sound attenuation capabilities of resonators and mufflers, providing essential guidelines for designing effective noise control devices [8].

Through this investigation, the author aims to provide a comprehensive understanding of how 90-degree duct elbows influence the acoustic behavior of helicoidal resonators.

The basic dimensions of the acoustic helicoidal resonator are presented in Fig. 1.

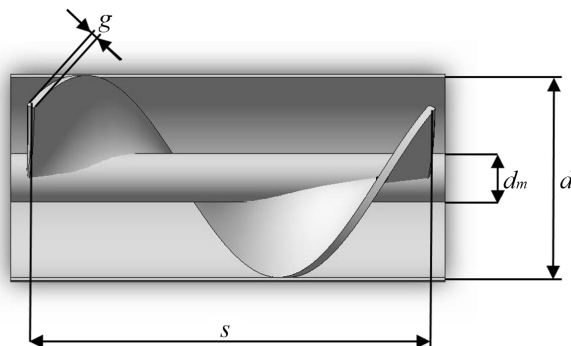


FIG. 1. Basic dimensions of an acoustic helicoidal resonator inside a cylindrical duct [17].

The considered acoustic system consists of a cylindrical duct with helicoidal resonator with the following characteristics:

- constant ratio between spiral lead s [m] to cylindrical duct diameter d [m], ratio $s/d = 1.976$,
- constant ratio of helicoidal profile thickness g [m] to cylindrical duct diameter d , ratio $g/d = 0.04$,
- constant ratio of cylindrical mandrel diameter d_m [m] to cylindrical duct diameter d , ratio $d_m/d = 0.24$.

2. COMPUTATIONAL ANALYSIS AND RESULTS

At the end of the helicoidal profile, a 90-degree duct elbow with a diameter of $d = 125$ mm was placed, relative to which the resonators were rotated around their axes. The duct elbow bend profile was characterized by a major radius d and a minor elbow radius $d/2$. In the numerical tests, the helicoidal profiles were rotated in 45° increments. An initial angle of 0° was established when the profile was placed at the highest position relative to the direction of the elbow bend, as presented in Fig. 2.

Three selected types of helicoidal resonators, with different numbers of turns ($n = 0.671$, $n = 0.695$, and $n = 1.0$) are associated with their specific TL

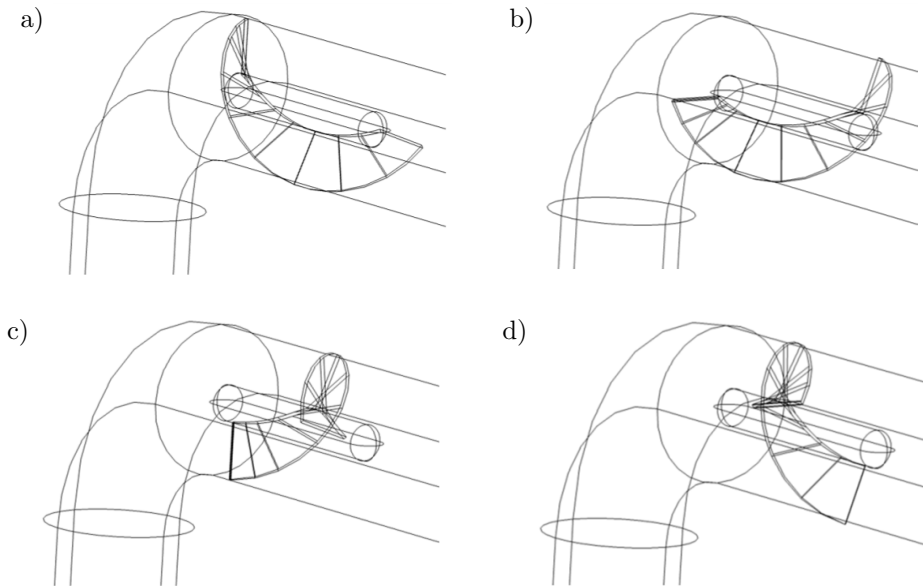


FIG. 2. Three-dimensional (3D) numerical visualization of the analyzed four rotation angles of helicoidal resonators relative to a 90-degree duct elbow: a) 0° ; b) 90° ; c) 180° ; d) 270° .

characteristics, as presented in Fig. 3. In this work, the frequency scale has been limited to the characteristic frequency range of the helicoidal resonator to highlight these difference.

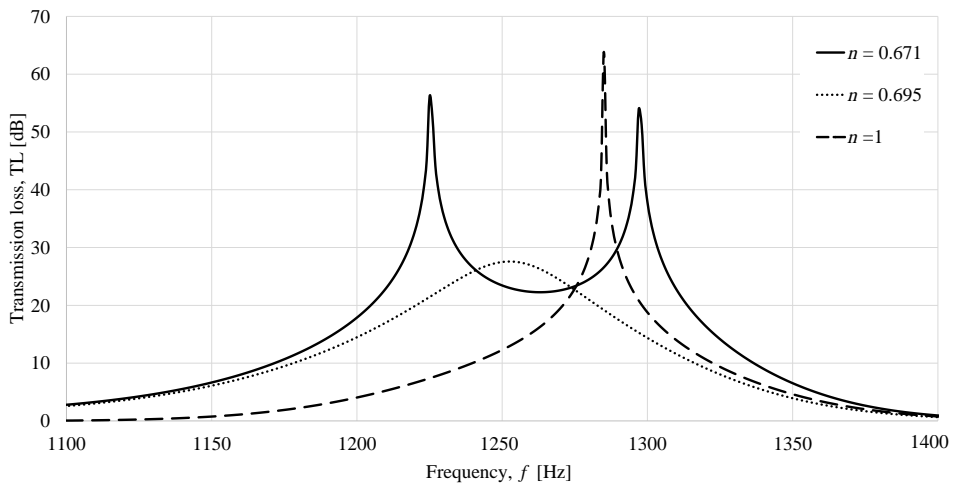


FIG. 3. Numerically obtained TL characteristics of three selected types of helicoidal resonators with a constant ratio $s/d = 1.976$ and different numbers of turns ($n = 0.671$, $n = 0.695$, and $n = 1.0$) placed in a straight cylindrical duct.

The helicoidal resonator with $n = 1.0$ is characterized by a single distinct resonance frequency. In contrast, the resonator with $n = 0.671$ exhibits two clearly identifiable resonance frequencies and relatively high TL between them.

A particularly unique feature is observed in the helicoidal resonator with $n = 0.695$, which does not exhibit a clearly defined resonance frequency like the other two. Instead, it represents an intermediate form between the resonators with $n = 0.671$ and $n = 1.0$, showing a smoother TL characteristic.

The observed difference in TL characteristics for helicoidal resonators with closely spaced numbers of helicoidal turns ($n = 0.671$ and $n = 0.695$) indeed suggests a strong sensitivity of the acoustic response to both geometric parameters and boundary conditions. These results highlight the non-linear and resonance-sensitive nature of the helicoidal resonator system, where small changes in the number of helicoidal turns can lead to significant changes in the coupling between resonator modes and the propagating acoustic wave.

Regarding generalization, while this study focuses on three specific values of n (0.671, 0.695, and 1.0), preliminary simulations indicate that the transmission characteristics evolve in a non-monotonic and geometry-sensitive manner with varying n . Therefore, while it is difficult to establish simple interpolation rules, the study does suggest that the numbers of helicoidal turns slightly below and above $n = 0.7$ may mark a transition between different dominant resonance mechanisms (e.g., between quarter-wave resonance and more distributed helical modal patterns).

The finite element method (FEM) was employed to solve 3D numerical models in the frequency domain by using time-harmonic pressure acoustics application mode in the COMSOL Multiphysics Acoustics Module computational application [3], as presented in Fig. 4.

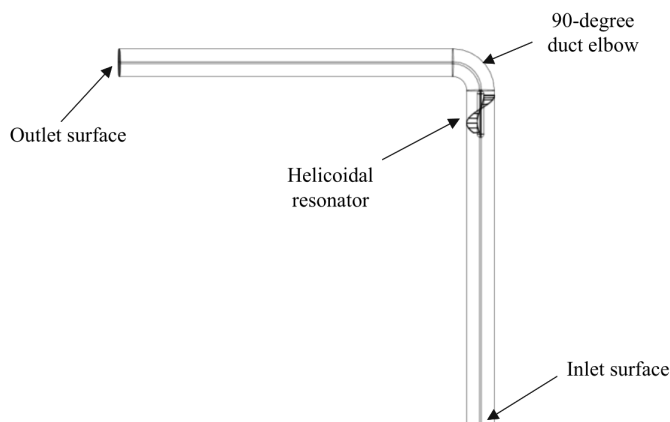


FIG. 4. Example 3D model of an acoustic duct system with a helicoidal resonator with ratio $s/d = 1.976$ and number of turns $n = 0.671$, and a 90-degree elbow at a 0-degree rotation angle.

The primary variable solved is the acoustic pressure p [Pa], which can be computed using the Helmholtz equation:

$$(2.1) \quad \nabla \cdot \left(-\frac{\nabla p}{\rho_0} \right) - \frac{\omega^2 p}{c_s^2 \rho_0} = 0,$$

where ρ_0 is the density of air ($\rho_0 = 1.23 \text{ kg/m}^3$), c_s is the speed of sound in air ($c_s = 343 \text{ m/s}$), and $\omega = 2\pi f$ gives the angular frequency, where f [Hz] denotes the frequency.

For the investigated models in this work, the boundary conditions are of three types [3]. For acoustically hard walls at the solid boundaries, which correspond to the walls of helicoidal profile, the mandrel and the cylindrical duct, the model uses sound-hard (wall) boundary conditions:

$$(2.2) \quad \left(\frac{\nabla p}{\rho_0} \right) \cdot \mathbf{n} = 0,$$

where \mathbf{n} is the normal direction vector of the investigated cylindrical duct.

The boundary condition at the inlet surface (sound source) of the cylindrical duct is a combination of incoming and outgoing plane waves:

$$(2.3) \quad \mathbf{n} \cdot \frac{1}{\rho_0} \nabla p + ik \frac{p}{\rho_0} + \frac{i}{2k} \Delta_T \frac{p}{\rho_0} = \left(\frac{i}{2k} \Delta_T \frac{p_0}{\rho_0} + (1 - (\mathbf{k} \cdot \mathbf{n})) ik \frac{p_0}{\rho_0} \right) e^{-ik(\mathbf{k} \cdot \mathbf{r})},$$

where Δ_T denotes the boundary tangential Laplace operator, $k = \omega/c_s$ is the wave number, \mathbf{n} is the natural direction vector for the investigated cylindrical duct, and the wave vector is defined as $\mathbf{k} = k\mathbf{n}_k$, where \mathbf{n}_k is the wave-direction vector. In Eq. (2.3), p_0 represents the applied outer pressure, and i denotes the imaginary unit. The inlet boundary condition is valid as long as the frequency is kept below the cutoff frequency for the second propagating mode in the cylindrical duct.

At the outlet boundary, a radiation boundary condition is applied to allow an outgoing wave to leave the modeling domain with minimal or no reflections:

$$(2.4) \quad \mathbf{n} \cdot \frac{1}{\rho_0} \nabla p + i \frac{k}{\rho_0} p + \frac{i}{2k} \Delta_T \frac{p}{\rho_0} = 0.$$

The numerical model is computed by the use of FEM, with element size chosen according to [20], and the maximum element size $h_e = 0.2 (c_s/f_{\max})$ [m], where f_{\max} [Hz] is the value of the maximum frequency investigated. Also, the longitudinal dimensions of the inlet and outlet cylindrical ducts are calculated as infinite by applying radiation boundary conditions.

The TL is used to evaluate the acoustic attenuation performance parameter [21, 25], and is given by:

$$(2.5) \quad \text{TL} = 10 \cdot \log_{10} \left[\frac{p_0^2}{|p_2|^2} \right] \text{ [dB]},$$

where p_0 is the maximum amplitude of the source sound pressure at the inlet, and p_2 is the maximum amplitude of the sound pressure at the outlet.

2.1. Number of helicoidal turns $n = 0.671$

Figure 5 presents the TL characteristics of a helicoidal resonator with a number of turns $n = 0.671$ for various rotation angles of a 90-degree duct elbow.

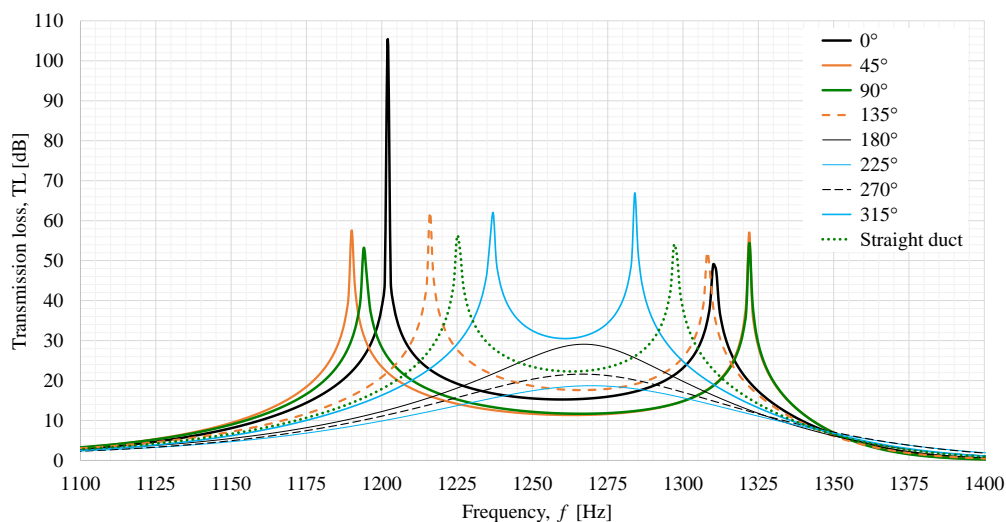


FIG. 5. TL characteristics of helicoidal resonators with $n = 0.671$, equipped with a 90-degree duct elbow at different rotation angles, compared to the TL characteristic of the same resonator in a straight duct.

For comparison, the TL characteristic of the same resonator placed in a straight cylindrical duct is also included in the figure.

In general, attaching a 90-degree elbow to the end of the helicoidal resonator causes a shift in the TL characteristics across the frequency domain.

Placing the elbow at a rotation angle of 0° results in a decrease of the first resonance frequency by approximately 23 Hz (to about 1202 Hz) and an increase of the second resonance frequency by about 13 Hz (to about 1310 Hz). Additionally, there is a reduction in TL of approximately 6 dB at the lowest point between the resonance frequencies compared to the straight-duct configuration.

Similar TL characteristics, with two distinct resonance frequencies, are observed for elbow rotation angles of 45° , 90° , 135° , and 315° . The greatest shift – lowering of the first resonance frequency by approximately 35 Hz (to about 1190 Hz) and increase of the second by about 25 Hz (to about 1322 Hz) – is obtained at a 45-degree rotation.

The smallest difference between the two resonance frequencies is observed at a 315° -degree angle, where the first resonance frequency increases by approximately 12 Hz, while the second decreases by about 26 Hz, along with an increase of approx. 8 dB in TL at the lowest point between the two resonance frequencies.

The remaining elbow rotation angles (180° , 225° , and 270°) produce TL characteristics similar to those of a helicoidal resonator with $n = 0.695$ placed in a straight cylindrical duct. However, the frequency corresponding to the peak TL, which reaches nearly 30 dB, is approximately 1265 Hz and occurs at a rotation angle of 180° . A rotation of 270° results in a reduction of TL at nearly the same frequency by about 7 dB. The lowest TL at the peak of the characteristic TL curve is observed at a rotation angle of 315° , with a value of approximately 19 dB at around 1270 Hz.

2.2. Number of helicoidal turns $n = 0.695$

Figure 6 presents the TL characteristics of a helicoidal resonator with a number of turns $n = 0.695$. Positioning the resonator at a rotation angle of 0° relative to the 90-degree duct elbow results in its TL characteristic very similar to that of a helicoidal resonator with $n = 0.671$ placed in a straight duct. In this case,

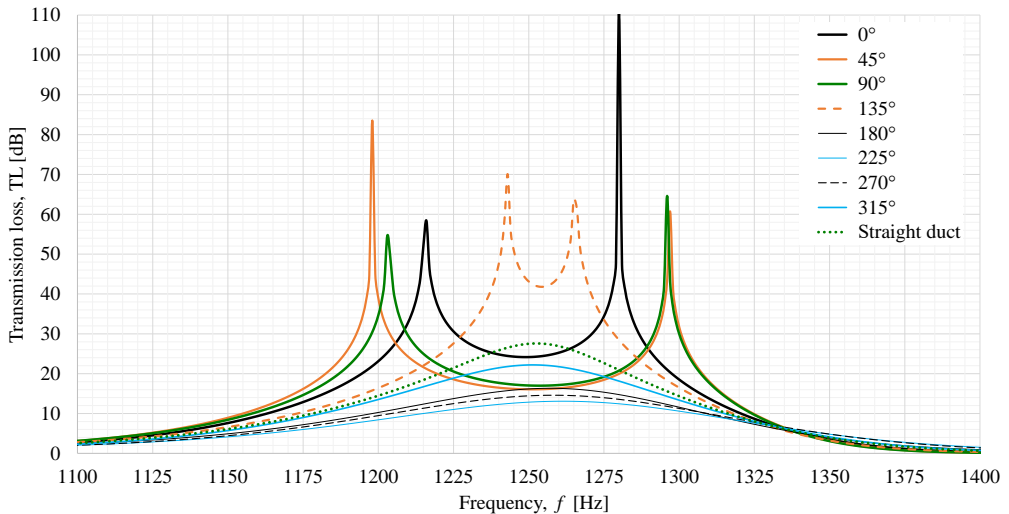


FIG. 6. TL characteristics of helicoidal resonators with $n = 0.695$ in a 90-degree duct elbow at different rotation angles compared to the TL characteristic in straight duct.

the TL at the lowest point between the two resonance frequencies is nearly identical, at approximately 24 dB. However, the first resonance frequency is about 10 Hz lower, approximately 1215 Hz, and the second resonance frequency is also lower by around 20 Hz, occurring at approximately 1280 Hz. The largest difference between the first and second resonance frequencies is observed at a rotation angle of 45° , while the smallest at 135° .

Thus, at rotation angles of 0° , 45° , 90° , and 135° , the TL characteristics exhibit a dual-resonance pattern. In contrast, at rotation angles of 180° , 225° , 270° , and 315° , the TL exhibits lower attenuation compared to that of the resonator placed in a straight cylindrical duct.

The frequency at which maximum attenuation occurs does not change significantly, remaining within the range from 1250 Hz (at 180°) to 1265 Hz (at 225°). At a rotation angle of 180° , the maximum TL reaches approximately 22 dB, while at 225° it is the lowest, around 13 dB. At 270° , the TL is approximately 14 dB, and at 315° , about 16 dB.

2.3. Number of helicoidal turns $n = 1.0$

Figure 7 presents the TL characteristics of a helicoidal resonator with a number of helicoidal turns $n = 1.0$ for various rotation angles relative to a 90-degree duct elbow.

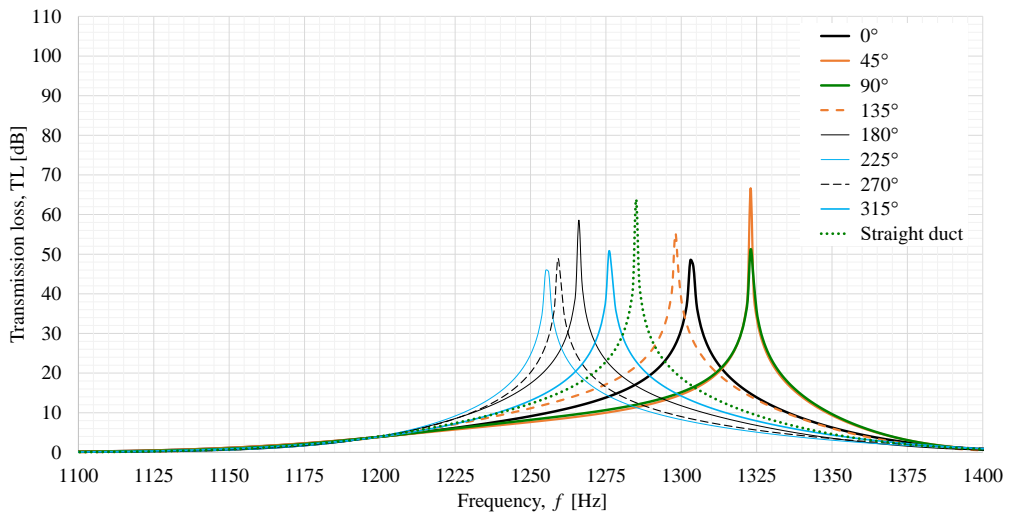


FIG. 7. TL characteristics of helicoidal resonators with $n = 1.0$ at a 90-degree duct elbow at different rotation angles, compared to the TL characteristic in a straight duct.

Positioning the elbow at a rotation angle of 0° increases the resonance frequency by approximately 18 Hz, reaching around 1303 Hz, compared to the TL

characteristic of the same helicoidal resonator placed in a straight duct. A nearly identical increase in resonance frequency is observed at rotation angles of 45° and 90° , with an increase of about 33 Hz to approximately 1323 Hz. At a rotation angle of 135° , the frequency increased by approximately 13 Hz to around 1298 Hz. In the remaining cases – at rotation angles of 180° , 225° , 270° , and 315° – a decrease in resonance frequency was observed.

The smallest decrease occurs at 315° , with a drop of about 10 Hz to approximately 1276 Hz. At 180° , the resonance frequency decreases by around 20 Hz, resulting in a frequency of approximately 1265 Hz. For a rotation angle of 270° , the frequency drops by 26 Hz to about 1259 Hz, and at 225° , the largest decrease is noted, with a drop of about 30 Hz to approximately 1250 Hz. In all cases, the TL at the resonance frequencies exceeds 45 dB.

3. EXPERIMENTAL ANALYSIS AND RESULTS

The three selected types of helicoidal resonators were manufactured for a duct with a diameter of 125 mm, a dimension commonly used in building ventilation systems. In the experimental tests, the helicoidal profiles were rotated every 90-degree increments. The initial rotation angle of 0° was adopted in the same way as in the numerical tests.

Figure 8 presents the experimental setup, which contains an isolated sound source connected to a 1-meter long pipe with a diameter of 125 mm, incorporating an acoustic helicoidal resonator at the end, a 90-degree elbow (standard type in the ventilation market) and a 0.86-meter long pipe at the outlet side oriented vertically. The measurement apparatus included a Bruel&Kjaer Pulse



FIG. 8. View of experimental setup with an isolated sound source connected to a 1-meter long pipe with a diameter of 125 mm, including an acoustic helicoidal resonator at the end, a 90-degree elbow (typical in the ventilation market), and a 0.86-meter long outlet pipe oriented vertically (side up).

system with a recommended free-field half-inch condenser microphone, along with a laptop running the Pulse Labshop system. The microphone was placed directly along the central axis of the outlet pipe surface cross section.

The room in which the measurement were conducted had dimensions of 7.2 m in width, 13 m in length, and 4.1 m in height. The average sound absorption coefficient of the room was about 0.41. The temperature was about 23°C, the relative air humidity equaled 43%, and the atmospheric pressure was about 1013 hPa. The outlet pipe was directed vertically (side-up), and the requirement to maintain a distance of at least 1 m from the wall was maintained to prevent sound distortion caused by reflections.

Figures 9–11 show the difference in sound pressure level (SPL difference [dB]) between the SPL spectra measured at the end of an acoustic system, consisting of empty pipes with a 90-degree elbow, and the system filled with the three analyzed helicoidal resonators at different rotation angles.

The SPL difference characteristics differ from the numerically obtained TL characteristics of helicoidal resonators presented in Figs. 5–7. This discrepancy is caused by the influence of the external environment, reflections from the dust inlets and outlets, as well as the effect of the acoustic wave propagating within the acoustic system – both internally and through lateral transmission. Despite all efforts to minimize these effects, they may have introduced some disturbances. Nevertheless, the calculated differences in acoustic pressure levels clearly indicate the sound attenuation achieved by all the analyzed helicoidal resonators and demonstrate how this attenuation varies with the rotation angle of the 90-degree duct elbow attached to their ends.

Figure 9 presents the acoustic pressure level differences for the resonator with a winding number of $n = 0.671$ at four different elbow rotation angles. At a rota-

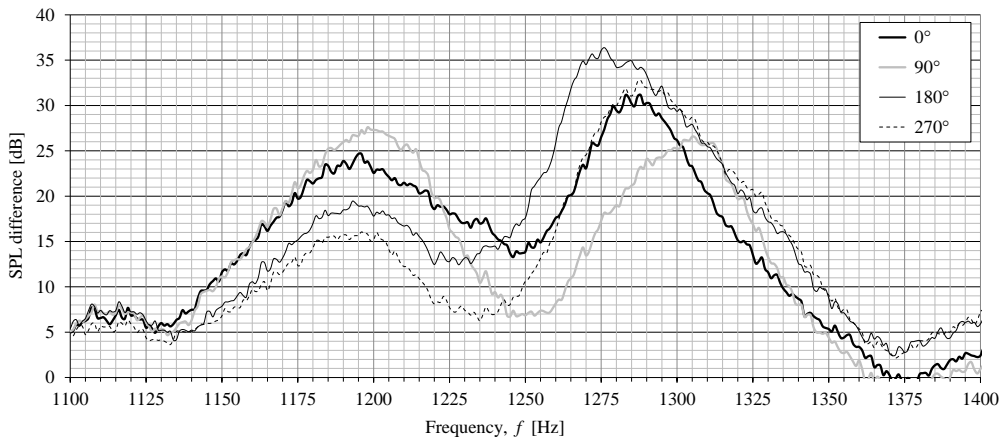


FIG. 9. SPL difference for the acoustic helicoidal resonator with $n = 0.671$ and a 90-degree duct elbow at different rotation angles.

tion angle of 0° , the highest sound attenuation occurs at approximately 1280 Hz. Compared to the numerical results (Fig. 4), this corresponds to a slightly lower second resonant frequency – by about 40 Hz. However, at a rotation angle of 90° , an increase in the second resonant frequency is observed, reaching 1305 Hz. Although this is still about 17 Hz lower than the numerical result, the trend of frequency shift aligns with the pattern observed in the numerical simulations. The difference between the highest second resonant frequencies at 0° and 90° in the experimental study is approximately 20 Hz, while in the numerical results it is around 12 Hz.

Unfortunately, the experimental data do not show a noticeable difference in the first resonant frequency between the 0- and 90-degree rotation angles – the peak values of the first resonant frequency are nearly identical in both cases. In contrast, numerical simulations indicate a decrease of about 7 Hz in the first resonant frequency at a 90-degree rotation compared to 0° . In Fig. 9, for rotation angles of 180° and 270° , a significant decrease in attenuation is observed at the first resonant frequency, while attenuation increases markedly in the region of the second resonant frequency. The numerical analysis (Fig. 4) did not reveal two distinct resonant frequencies for these rotation angles; instead, a single broad peak in the TL curve was observed. Nevertheless, the attenuation value at a 180-degree rotation is clearly higher than that at 270° , a trend also confirmed by the experimental results. Moreover, there is a strong correspondence in the frequency at which maximum attenuation occurs. For the 180-degree angle in the numerical study, this frequency is approximately 1265 Hz – with the strongest attenuation range between approximately 1260 Hz and 1275 Hz. In the experimental results, this range shifts slightly higher, from about 1265 Hz to 1285 Hz. Thus, the difference in the frequency at which maximum attenuation occurs between the numerical and experimental data is relatively small.

Figure 10 presents the differences in acoustic pressure levels for the resonator with a number of helicoidal turns $n = 0.695$ equipped with a 90-degree elbow, analyzed at four rotation angles: 0° , 90° , 180° , and 270° . At the 0° and 90° rotation angles, pronounced sound attenuation is observed at both the first and second resonant frequencies. Compared to the numerical simulation results, the experimental attenuation characteristics exhibit a similar trend. Specifically, the attenuation at the first resonant frequency is noticeably lower in the experiments, while it increases significantly at the second resonant frequency.

At a 90° rotation, the first resonant frequency coincides with that observed at 0° . However, the second resonant frequency at 90° is slightly higher than at 0° , which is consistent with the numerical results, where a difference of approximately 15 Hz was predicted. Moreover, the values of the second resonant frequency show strong agreement between experiment and simulation: for the 0° angle,

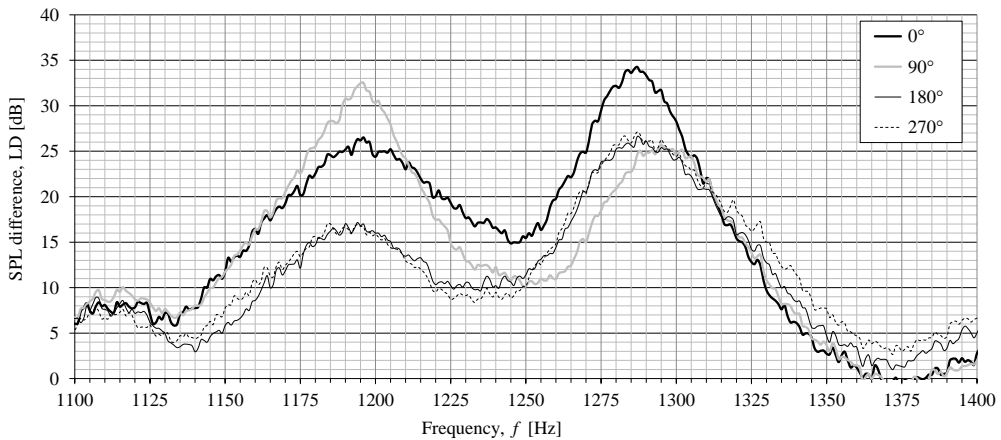


FIG. 10. SPL difference for the helicoidal resonator with $n = 0.695$ and a 90-degree duct elbow at different rotation angles.

the experimental value is approximately 1282 Hz, closely matching the simulated result of 1281 Hz. Similarly, at 90°, the second resonant frequency measured experimentally is about 1295 Hz, while the numerical result is 1291 Hz – demonstrating a high level of consistency.

For the 180° and 270° rotation angles, lower sound attenuation values were obtained, which also aligns with the numerical findings. In these cases, the first resonant frequency is less clearly defined, but a distinct increase in attenuation – by approximately 10 dB – is observed in the region of the second resonant frequency.

The SPL difference characteristics for the 180° and 270° rotations are very similar to each other in the experimental data. Interestingly, the numerical simulations also show only minor deviations between these two rotation angles. Additionally, the magnitude of sound attenuation in the second resonant frequency region is relatively modest: around 26 dB in the numerical simulations and approximately 16 dB–17 dB in the experimental results.

Figure 11 shows the acoustic pressure level difference characteristics for the helicoidal resonator with a number of helicoidal turns $n = 1$, equipped with a 90-degree elbow, analyzed at four rotation angles: 0°, 90°, 180°, and 270°. A particularly notable feature is the high degree of qualitative consistency in the distribution between the experimentally recorded pressure difference curves and the TL characteristics obtained from numerical simulations.

The highest resonant frequency, in both experimental and numerical results, was observed at a rotation angle of 90°, while the lowest was recorded at 270°. As in the numerical simulations, the difference in resonant frequency between the 270° and 180° angles is small – approximately 10 Hz in the experimental

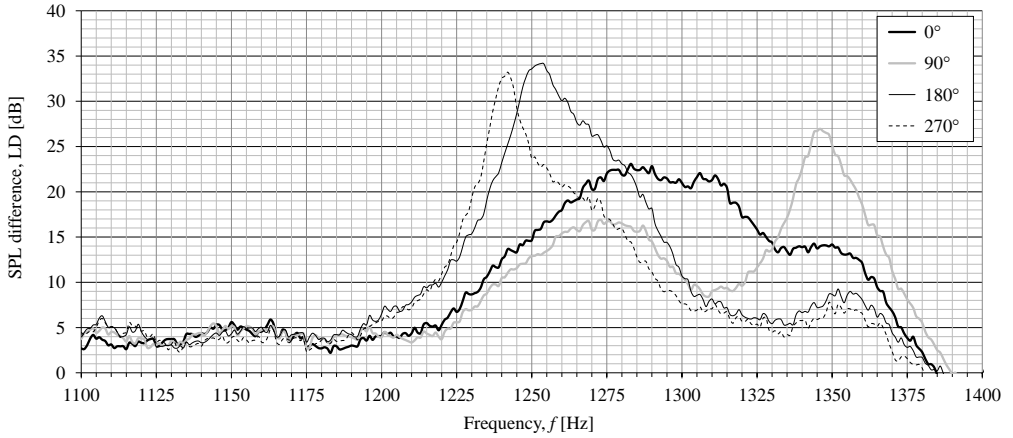


FIG. 11. SPL difference for the helicoidal resonator with $n = 1.0$ and a 90-degree duct elbow at different rotation angles.

data and around 7 Hz in the numerical results. Specifically, in the experiment, the resonant frequency at 180° is approximately 1254 Hz, and at 270° it is about 1242 Hz. In contrast, the corresponding numerical results yield slightly higher values: approximately 1266 Hz for 180° and 1259 Hz for 270° .

For the 0° rotation angle, no distinct resonant peak is observed in the experimental data. Instead, a broader frequency band of enhanced attenuation can be identified, ranging from approximately 1265 Hz to 1315 Hz, with attenuation levels exceeding 20 dB. In the numerical simulations, however, the resonant frequency at 0° is clearly defined at around 1303 Hz (Fig. 7).

In the experimental results for the 90° rotation, the resonant frequency is clearly visible at approximately 1345 Hz, although its magnitude is slightly lower than that predicted by the simulations, which indicated a value around 1323 Hz.

4. CONCLUSIONS

This study presented the results of numerical and experimental analyses focused on the tuning behavior of three types of acoustic helicoidal resonators, all sharing the same geometric ratio ($s/d = 1.976$) but differing in the number of helicoidal turns: $n = 0.671$, 0.695 , and 1.0 . Tuning was achieved by attaching a 90-degree duct elbow and varying its angular orientation relative to the resonator axis.

The numerical results, expressed as TL characteristics, clearly indicated that both the presence and angular orientation of the elbow significantly influence the acoustic response of the resonators. For the resonators with $n = 0.671$ and $n = 0.695$, substantial changes were observed in both the number and position of

the resonant frequencies, with some configurations exhibiting a single dominant resonance, while others showed two. In contrast, the resonator with $n = 1.0$ consistently exhibited a single resonance, which shifted in frequency depending on the rotation angle of the elbow.

The experimental measurements confirmed the general trends predicted by the numerical simulations, particularly with regard to the shifting of resonant frequencies and variations in sound attenuation levels. Although minor discrepancies in frequency values and attenuation magnitudes were observed – mainly due to environmental factors, acoustic reflections, side radiation and slight differences in the shape of the 90-degree elbow profile – the overall correlation between the numerical and experimental data was strong.

These findings support the conclusion that helicoidal resonators can be effectively tuned by altering their orientation relative to a 90-degree duct elbow. This tuning results in controlled shifts of resonance frequencies and corresponding changes in the sound attenuation characteristics of the system. Such a configuration offers a practical and passive method for adaptive noise control in ducted acoustic environments.

Future work should expand this investigation to include other types of common geometric perturbations in duct systems, such as *Y*-branches, *T*-junctions, or smooth-radius bends, in order to evaluate the generalizability of the tuning mechanism and to develop design guidelines for optimized acoustic performance in more complex systems.

This study is limited to three specific values of the number of helicoidal turns ($n = 0.671$, 0.695 , and 1.0), and the resonators were analyzed in combination with a 90-degree duct elbow at discrete angular positions. While these configurations provide valuable insight into the coupling between geometrical parameters and acoustic TL, the results may not directly generalize to other helicoidal turn values, duct geometries, or boundary conditions.

Additionally, the experimental setup, although carefully constructed, may introduce minor deviations due to manufacturing tolerances and imperfect alignment. Numerical simulations, on the other hand, rely on idealized boundary conditions and do not fully account for viscous or thermal losses, which may contribute to the observed discrepancies between measured and simulated data. Further studies are necessary to map a broader parameter space and to perform sensitivity analyses that account for uncertainties in geometry and material properties

FUNDING

This work was financed by the Polish Ministry of Science and Higher Education under research project no. 0612/SBAD/3628.

REFERENCES

1. CHANAUD R., Effects of geometry on the resonance frequency of Helmholtz resonators, *Journal of Sound and Vibrations*, **178**: 337–348, 1994, <https://doi.org/10.1006/jsvi.1994.1490>.
2. CHENG Y., TINGSHENG Z., JIAXING L., SHUTING Y., SHIJUN Y., HONGCHANG Z., ZHIWEI Z., Extended tube acoustic metamaterial: Its modeling and application to a kitchen hood, *Applied Acoustics*, **185**: 108398, 2022, <https://doi.org/10.1016/j.apacoust.2021.108398>.
3. COMSOL A.B., *Comsol Multiphysics, Acoustics Module, User's Guide and Model Library*, Documentation Set, Stockholm, Sweden, 2020.
4. GAUTAM A., CELIK A., AZARPEYVAND M., An experimental and numerical study on the effect of spacing between two Helmholtz resonators, *Acoustics*, **3**(1): 97–117, 2021, <https://doi.org/10.3390/acoustics3010009>.
5. GULCAN A., SAIT E.S., Breaking the limits of acoustic science: A review of acoustic metamaterials, *Materials Science & Engineering B*, **305**: 117384, 2024, <https://doi.org/10.1016/j.mseb.2024.117384>.
6. GUO J., ZHANG X., FANG Y., JIANG Z., Wideband low-frequency sound absorption by inhomogeneous multi-layer resonators with extended necks, *Composite Structures*, **260**: 113538, 2021, <https://doi.org/10.1016/j.compstruct.2020.113538>.
7. HU Z., YANG C., CHENG L., Acoustic resonator tuning strategies for the narrowband noise control in an enclosure, *Applied Acoustics*, **134**: 88–96, 2018, <https://doi.org/10.1016/j.apacoust.2018.01.013>.
8. KHAIRUDDIN M.H., SAID M.F.M., DAHLAN A.A., KADIR K.A., Review on resonator and muffler configuration acoustics, *Archives of Acoustics*, **43**(3): 369–384, 2018, <https://doi.org/10.1134/S1063771017030071>.
9. KOMKIN A.I., MIRONOV M.A., BYKOV A.I., Sound absorption by a Helmholtz resonator, *Acoustical Physics*, **63**: 385–392, 2017, <http://doi.org/10.1134/S1063771017030071>.
10. LANGFELDT F., HOPPEN H., GLEINE W., Broadband low-frequency sound transmission loss improvement of double walls with Helmholtz resonators, *Journal of Sound and Vibrations*, **476**: 115309, 2020, <https://doi.org/10.1016/j.jsv.2020.115309>.
11. LV C., WANG X., MEI Y., Optimization method of acoustic filter structures composed of Helmholtz resonators based on genetic algorithm, *Journal of Physics: Conference Series*, **2467**(1): 012005, 2023, <https://doi.org/10.1088/1742-6596/2468/1/012019>.
12. ŁAPKA W., Acoustic attenuation performance of a round silencer with the spiral duct at the inlet, *Archives of Acoustics*, **32**(4S): 247–252, 2007.
13. ŁAPKA W., *Acoustical properties of helicoid as an element of silencers*, Ph.D. Thesis, Faculty of Mechanical Engineering and Management, Poznań University of Technology, 2009.
14. ŁAPKA W., CEMPEL C., Acoustic attenuation performance of Helmholtz resonator and spiral duct, *Vibrations in Physical Systems*, **23**: 247–252, 2008.
15. ŁAPKA W., Numerical analysis of sound propagation in selected acoustical system with helicoidal resonator placed in cylindrical duct with 90 degree elbow, *Vibrations in Physical Systems*, **29**: 2018018, 2018, http://vibsys.put.poznan.pl/_journal/2018-29/articles/vibsys_2018018.pdf.

16. ŁAPKA W., A three-dimensional finite element analysis of tuning the selected acoustic helicoidal resonator by the change of its mandrel diameter, *Applied Acoustics*, **185**: 108443, 2022, <http://doi.org/10.1016/j.apacoust.2021.108443>.
17. ŁAPKA W., JAKUBOWSKI P., Experimental and CFD study of the selected acoustic helicoidal resonator as a final element of an air installation, *Vibrations in Physical Systems*, **34**(1): 2023112, 2023, <http://doi.org/10.21008/j.0860-6897.2023.1.12>.
18. ŁAPKA W., JAKUBOWSKI P., Experimental aeroacoustic studies of selected three types of helicoidal resonators, *Vibrations in Physical Systems*, **35**(1): 2024102, 2024, <http://doi.org/10.21008/j.0860-6897.2024.1.02>.
19. MA G., SHENG P., Acoustic metamaterials: From local resonances to broad horizons, *Science Advances*, **2**(2): e1501595, 2016, <https://doi.org/10.1126/sciadv.1501595>.
20. MARBURG S., NOLTE B., *Computational Acoustics of Noise Propagation in Fluids – Finite and Boundary Element Methods*, Springer-Verlag, Berlin, Germany, 2008.
21. MUNJAL M.L., *Acoustics of Ducts and Mufflers with Application to Exhaust and Ventilation System Design*, John Wiley & Sons, Calgary, Canada, 1987.
22. SELAMET A., LEE I.J., Helmholtz resonator with extended neck, *Journal of the Acoustical Society of America*, **113**: 1975–1985, 2003, <https://doi.org/10.1121/1.1558379>.
23. SHI X., MAK C.M., Helmholtz resonator with a spiral neck, *Applied Acoustics*, **99**: 68–71, 2015, <https://doi.org/10.1016/j.apacoust.2015.05.012>.
24. TANG S.K., On Helmholtz resonators with tapered necks, *Journal of Sound and Vibrations*, **279**: 1085–1096, 2005, <https://doi.org/10.1016/j.jsv.2003.11.032>.
25. VER I.L., BERANEK L.L., *Noise and Vibration Control Engineering*, 2nd ed., Hoboken, John Wiley & Sons, New Jersey, USA, 2005.
26. XUE R., MAK C.M., WU D., MA K.W., The acoustic performance of a dual Helmholtz resonators system in the presence of a grazing flow, *International Journal of Aeroacoustics*, **22**(1–2): 23–40, 2023, <https://doi.org/10.1177/1475472X221150175>.

Received June 27, 2025; accepted version August 21, 2025.

Online first December 2, 2025.
